ELSEVIER

Ceramics International 30 (2004) 773–783

CERAMICS INTERNATIONAL

www.elsevier.com/locate/ceramint

Oxidation behavior of AlN–Al_2O_3 composites

A. Maghsoudipour [a,*], F. Moztarzadeh [a], M. Saremi [b], J.G. Heinrich [c]

[a] *Ceramics Department, Materials and Energy Research Center, P.O. Box 14155-4777, Tehran, Iran*
[b] *Metallurgy and Materials Department, Tehran University, Tehran, Iran*
[c] *Technical University Clausthal, Germany*

Received 7 April 2003; received in revised form 16 September 2003; accepted 2 October 2003

Available online 19 March 2004

Abstract

The effect of composition and microstructure on the oxidation behavior of AlN samples having different amounts of Al_2O_3 was investigated. Oxidation was studied by weight gain measurement in air at elevated temperatures up to 1300 °C using an analytical balance.

The microstructure of sintered samples was characterized by scanning electron microscope and optical microscopy. The results showed that presence of different phases and microstructure have a great influence on the oxidation behavior of sintered AlN–Al_2O_3 composites. Samples having 1 wt.% alumina could not produce protective oxide layer around them and consequently the whole sample was oxidized to Al_2O_3. However, around the samples having 20 and 70 wt.% alumina a protective oxide layer was formed which retarded their further oxidation.

Keywords: B. Composites; C. Corrosion; D. Al_2O_3; AlN; Oxidation

1. Introduction

Many researchers [1–8] who have investigated the oxidation behavior of aluminum nitride and aluminum oxynitride in various environments have reported different results because the oxidation process was affected by parameters such as: particle size, temperature, carbon impurity and the humidity of environment [1]. Kim and Moorhead [3] reported that at temperatures below 1200 °C a linear weight gain is obtained on sintered aluminum nitride while at higher temperature the weight gain became parabolic. Barthelme et al. [5] reported a parabolic kinetics for oxidation of AlN ceramics between 1100 and 1400 °C.

The oxidation of AlN and γ-AlON involves the loss of nitrogen [3,9] according to the following equation:

$$4Al_{23}O_{27}N_5 + 15O_2 \rightarrow 46Al_2O_3 + 10N_2$$

$$4AlN + 3O_2 \rightarrow 2Al_2O_3 + 2N_2$$

During the oxidation of γ-AlON, in air at 1200 °C, a protective oxide layer can form around the sample. However, in pure oxygen atmosphere the oxidation process starts from 650 °C and the protective oxide layer does not form [9].

The aim of this work is to studying the influence of microstructure and composition on the oxidation behavior of different AlN–Al_2O_3 system composites.

2. Experimental procedure

Samples with different composition, selected from different areas of the equilibrium phase diagram of AlN–Al_2O_3 system (Fig. 1), were nominated as: A, B, C, and D. Samples were formed by isostatic pressing of the constituting powders, sintered in a gas pressure furnace at different sintering temperatures in nitrogen atmosphere. Details of the sintering processes have been published in the previous paper [10]. Table 1 shows the composition, sintering temperature, and relative density of the sintered samples.

During oxidation process samples were put on alumina tubes (Fig. 2) in order to have both sides of the samples in contact with air at high temperatures.

Oxidation behavior of sintered samples was studied at temperature range of 1100–1300 °C by measuring the weight gains (ΔM) using an analytical balance with a sensitivity of 0.1 mg. The weight gain (ΔM) was converted into relative

* Corresponding author. Tel.: +98-261-6204131; fax: +98-21-8773352.
E-mail address: a-maghsoudi@merc.ac.ir (A. Maghsoudipour).

0272-8842/$30.00
doi:10.1016/j.ceramint.2003.10.004

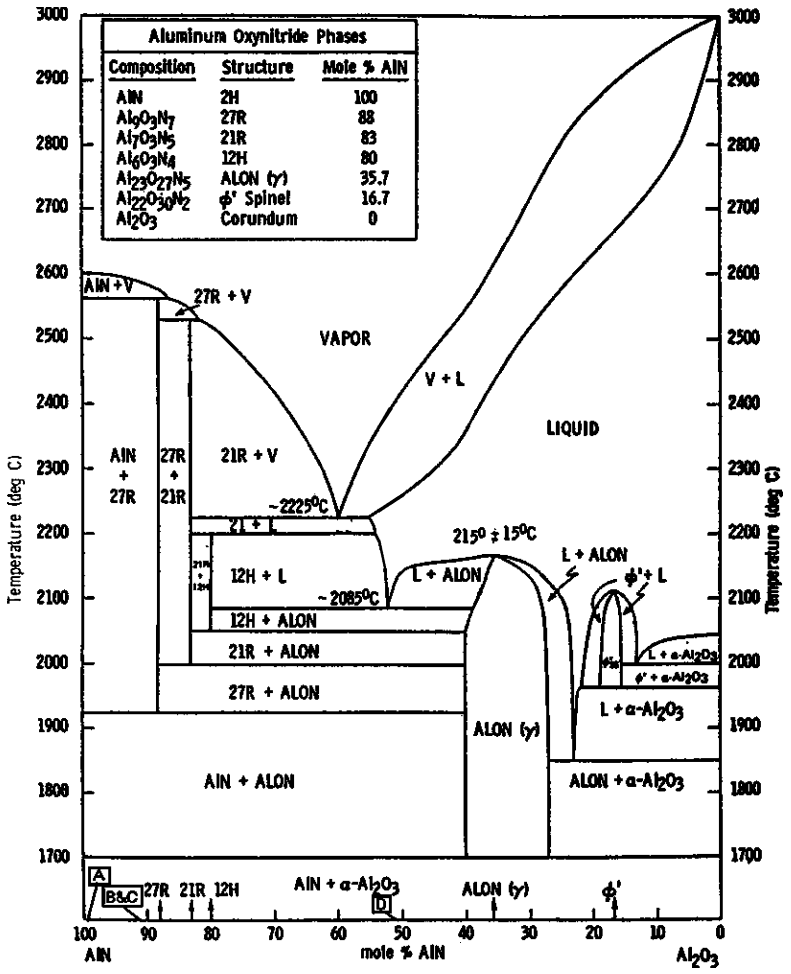

Fig. 1. Phase equilibrium diagram for the AlN–Al_2O_3 system [9].

Table 1
Technical data of experimental samples

Sample code	Composition[a]		Sintering temperature (°C)	Relative density (%)
	AlN	Al_2O_3		
A	99	1	1900	100
B	80	20	1800	93
C	80	20	1900	90
D	30	70	1850	100

[a] All samples contained Y_2O_3 with a weight ratio of Y_2O_3/AlN = 2.

weight gain (ΔM_r), using equation:

$$\Delta M_r = \left(\frac{\Delta M}{A \times \Delta M^*}\right) \times 2.4$$

where ΔM^* is theoretical weight gain corresponding to complete oxidation of the samples (calculated by semi-quantitative XRD analysis data), A is the surface area of the sample and 2.4 is a correction factor. During the oxidation processes two phenomena can take place concurrently; a weight gain as a result of oxidation and a weight

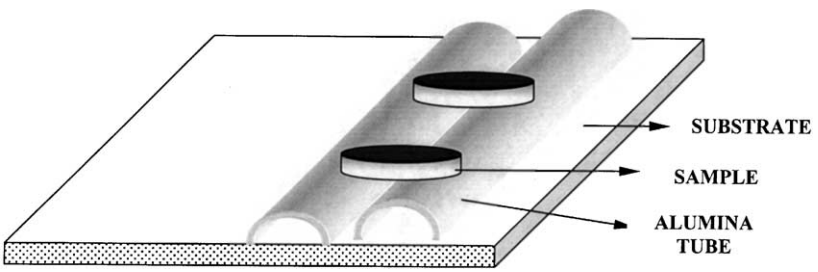

Fig. 2. Setting of the samples on the alumina tubes in the furnace.

loss because of nitrogen release. Hence, the net weight gain of the oxidation can be calculated by multiply ΔM by 2.4.

After oxidation process polished and fractured surfaces were examined with optical and scanning electron microscopy. Weight percent of different phases were measured by XRD technique using internal standard method and SiO_2 as the reference. The results of semi-quantitative phase analysis of sintered samples are listed in Table 2.

Table 2
Semi-quantitative phase analysis of sintered samples

	Sample A	Sample B	Sample C	Sample D
AlN (wt.%)	95 ± 5	73 ± 3	71 ± 3	20 ± 4
γ-AlON (wt.%)	5 ± 1	27 ± 5	16 ± 4	80 ± 7
27R (wt.%)	0	0	13 ± 7	0

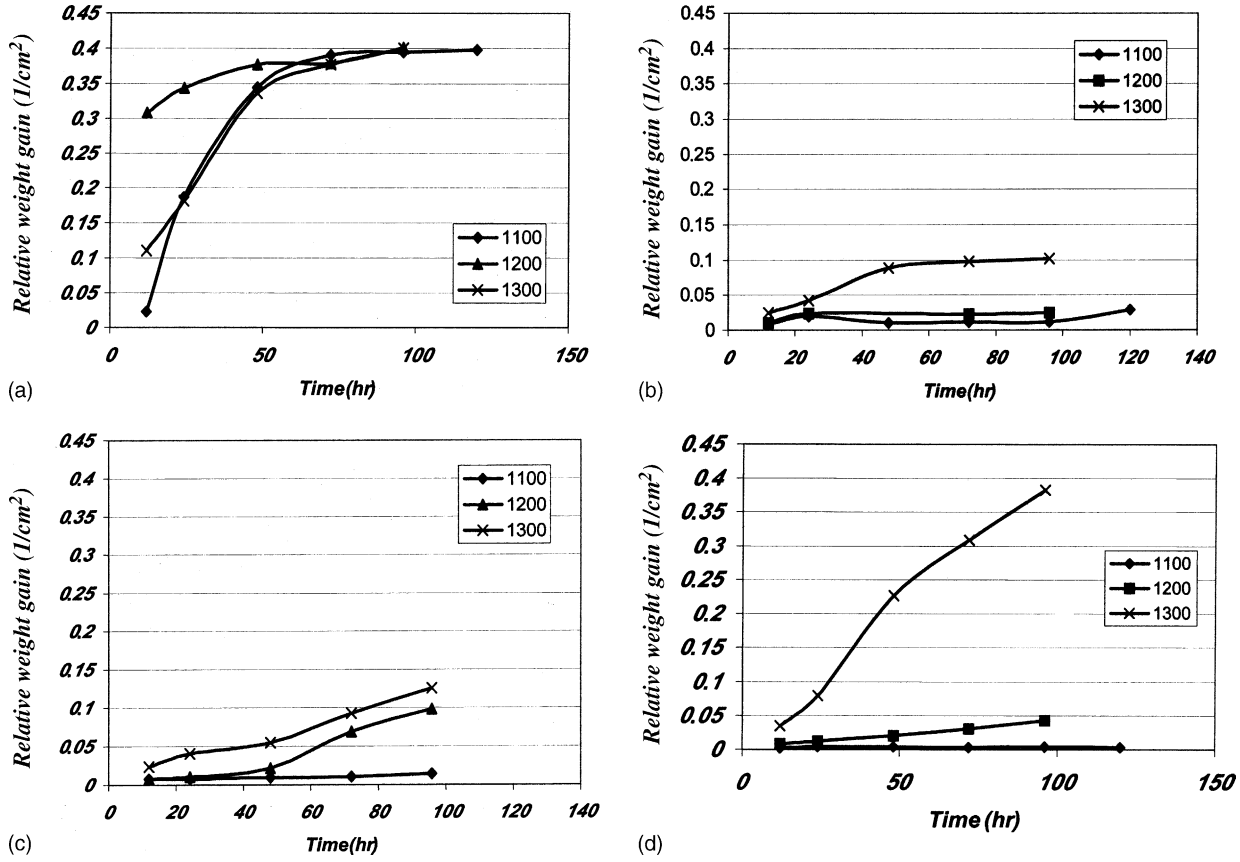

Fig. 3. Relative weight gain vs. exposure time: (a) sample A, (b) sample B, (c) sample C and (d) sample D.

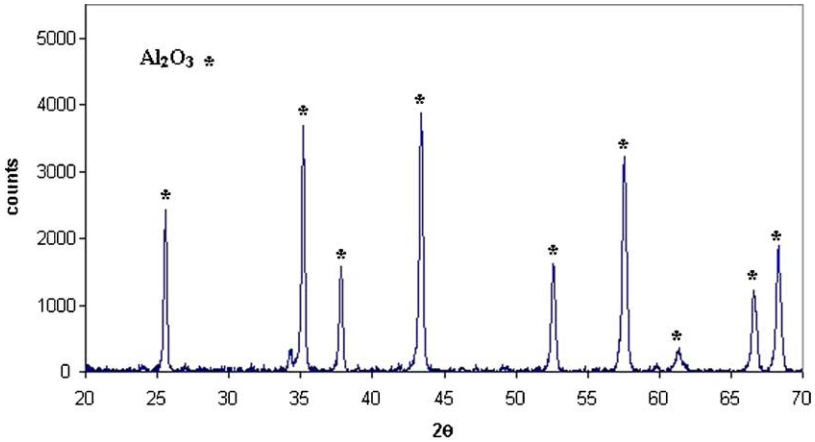

Fig. 4. XRD pattern of the sample A after oxidation at 1100 °C for 96 h.

3. Results and discussion

Relative weight gain of the specimens oxidized at 1100, 1200, and 1300 °C at various periods of time are shown in Fig. 3. The results show that sample A with 1 wt.% alumina, that was oxidized for 96 h at 1100 °C, had a low oxidation resistance and was converted completely to Al_2O_3. Its XRD analysis shown in Fig. 4 indicates full Al_2O_3 pattern. Samples B and C, both with 20 wt.% alumina, showed the best oxidation resistance while sample D with 70 wt.% alumina was better than sample A still lower than sample B and C. Comparison of the phase compositions in Table 2 and their relative weight gains in Fig. 3 showed that the phase composition is not a major factor affecting the oxidation behavior of the specimens. Samples A and D, with the same com-

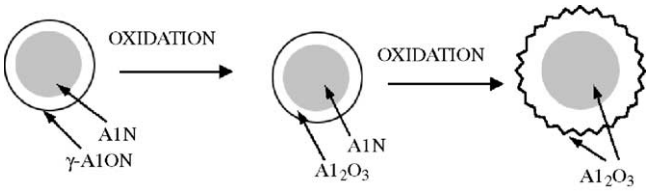

Fig. 6. Schematic diagram of the oxidation processes for the sample A.

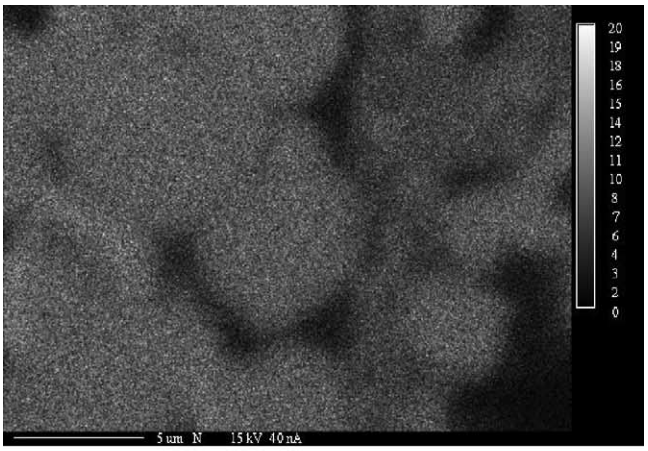

(a)

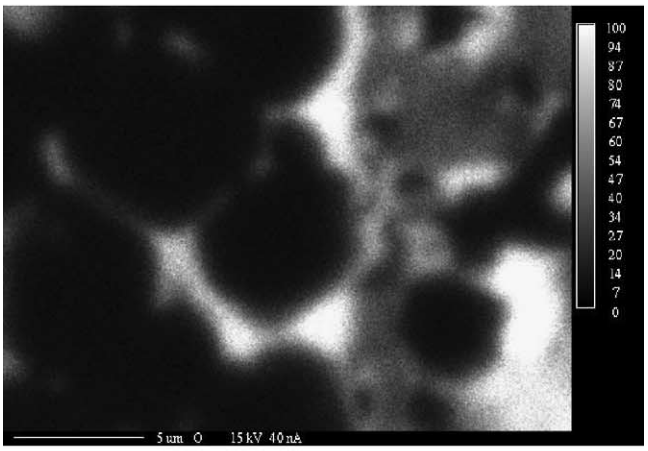

(b)

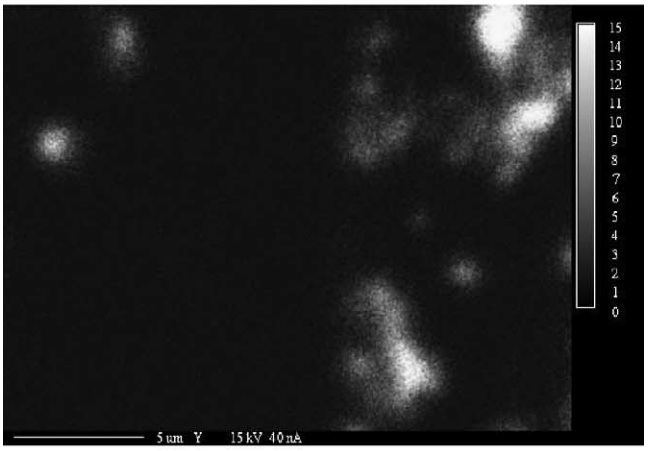

(c)

Fig. 5. WDS dot map of the sample A: (a) nitrogen map, (b) oxygen map and (c) yttrium map.

Fig. 7. SEM micrograph of polished section of the sample A oxidized at 1100 °C for 96 h.

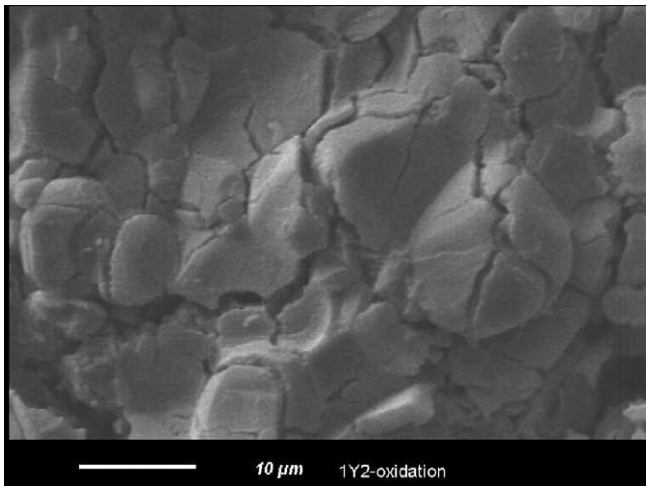

Fig. 8. SEM micrograph of fractured surface of sample A oxidized at 1100 °C for 96 h.

position but with high and low amount of AlN phase, respectively, did not show similar oxidation resistance, which may be interpreted that the effect of microstructure is more significant.

Distribution of the constituting elements; N, O, and Y in sample A are shown by their X-ray dot maps in Fig. 5. Distribution of AlN grains in the sample is illustrated through its nitrogen map in Fig. 5a, while the oxygen map (Fig. 5b) is an indicator of γ-AlON ($Al_{23}O_{27}N_5$) phase and additionally shows that AlN grains are surrounded by the γ-AlON phase. The yttrium map in Fig. 5c shows that the YAG phase ($Al_5O_{12}Y_3$) is distributed in triple points. It can be understood from Fig. 5 that most of the AlN grains are surrounded by γ-AlON phase, which was converted to Al_2O_3, during the oxidation process. Additionally, a dense oxide layer was also formed around AlN grains. Further oxidation causes AlN grains to be converted to Al_2O_3 according to the following equation too [2]:

$$2AlN + \frac{3}{2}O_2 \rightarrow Al_2O_3 + N_2$$

During the oxidation of aluminum nitride a lot of nitrogen gas was evolved from inside the sample which could not exit through the dense oxide layer around the AlN grains. Consequently, the increased gas pressure could break the oxide layer around the AlN grains and sample was expanded by formation of expansive cracks and channels within it. These cracks and channels will accelerate the transport of oxygen and nitrogen in the specimen developing its fast oxidation. The schematic figure of this process for sample A is illustrated in Fig. 6.

The comparison of the SEM micrographs of polished and fractured section of sample A (Figs. 7 and 8) indicates that no protective oxide has formed around the sample. That means

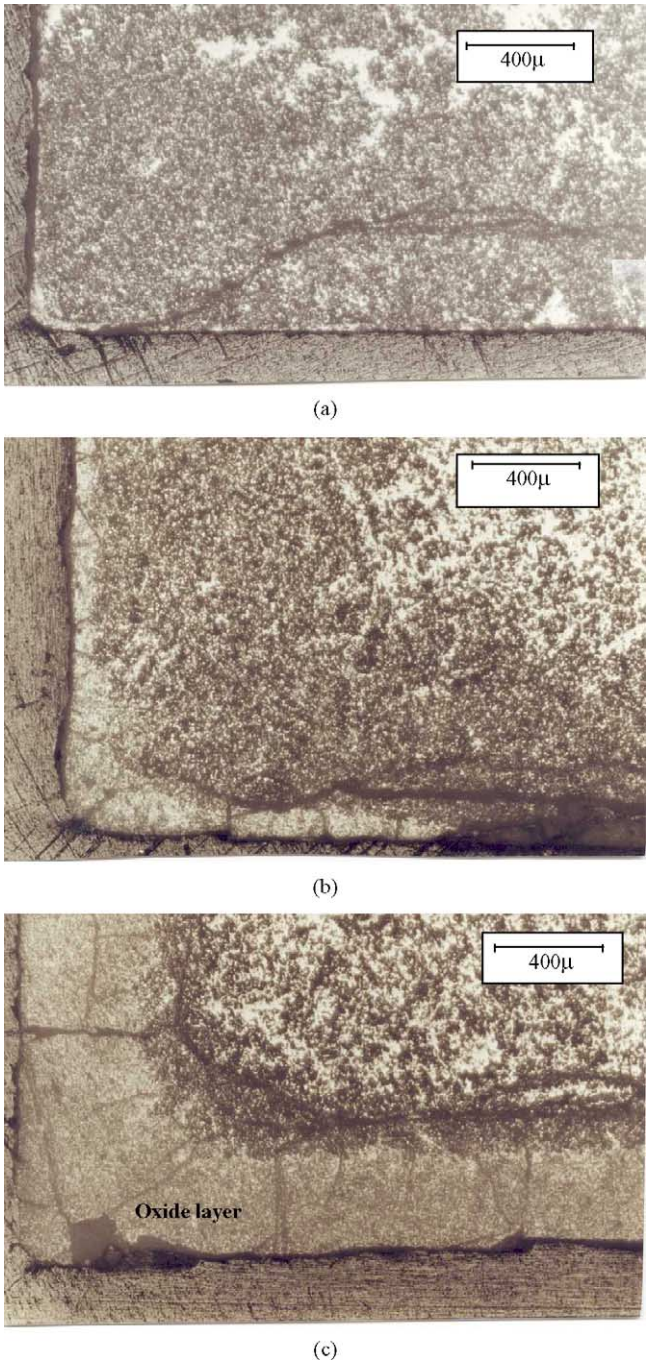

Fig. 9. Optical micrographs of polished section of the sample B oxidized at: (a) 1100 °C, 120 h, (b) 1300 °C, 12 h and (c) 1300 °C, 96 h.

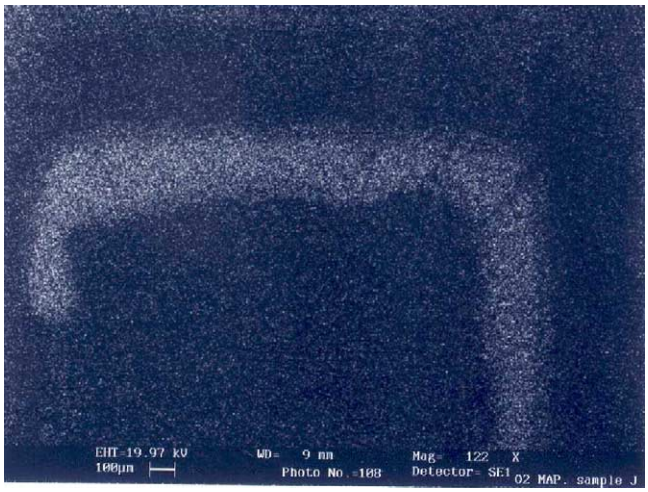

Fig. 10. Oxygen map of the sample B oxidized at 1300 °C for 96 h.

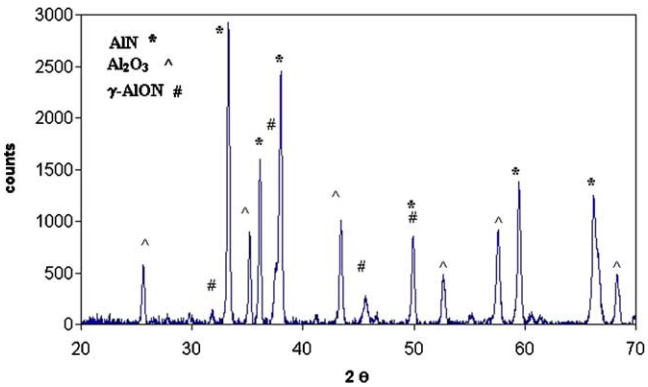

Fig. 11. XRD pattern of the sample B oxidized at 1300 °C for 96 h.

due to the expansive cracking around the AlN grains the sample was fully oxidized to alumina. In contrast, the optical micrographs of the polished section of sample B in Fig. 9 show that a thick oxide layer has formed around the sample B which thickens by increasing oxidation temperature and exposure time. The oxygen X-ray map obtained by WDS analysis (Fig. 10) showed the distribution of oxygen in this layer. The XRD analysis (Fig. 11) confirmed the formation of Al_2O_3 in this layer that protects the rest of the sample from oxidation.

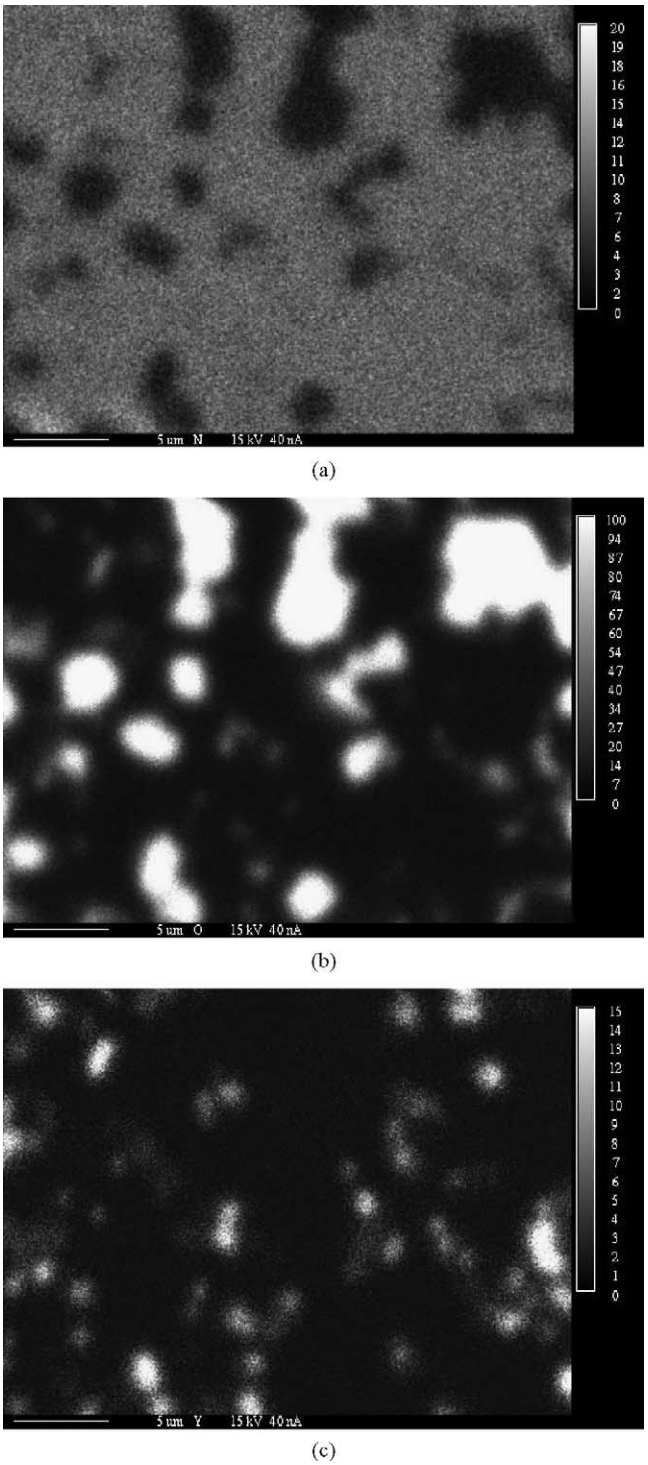

Fig. 12. WDS dot map of the sample B: (a) nitrogen map, (b) oxygen map and (c) yttrium map.

Samples A and B are microstructurally different. The nitrogen map of sample B (Fig. 12a) shows that AlN is a continuous background phase. Oxygen map and yttrium map (Fig. 12b and c) show that γ-AlON and YAG phases (white area) are distributed in this matrix as isolated phases.

Semi-quantitative XRD phase analysis (Table 2) shows that AlN is the major constituent phase (73 wt.%) and γ-AlON is the minor phase (27 wt.%) and are distributed separately. Hence, the oxidation of γ-AlON phase does not affect the oxidation of the AlN and no expansive cracking were observed such as those seen in sample A.

During the oxidation of sample B the evolved nitrogen gas was escaped from low resistance paths, such as grain boundaries, then a stable oxide layer was formed around the sample. This layer could protect it from further oxidation and the growth of this oxide layer controlled the oxidation rate of the specimen.

It is not feasible to fit a complete kinetic law of oxidation under such experimental condition of 6-point measurement (12, 24, 48, 72, 96, and 120 h). But it seems that the oxidation behavior of sample B (Fig. 3) is closed to a parabolic rate law, mainly formation of a protective Al_2O_3 layer on its surface.

The starting formulation of sample B and sample C was the same but sample C had different microstructure because of its high sintering temperature. Formation of 27R phase at high sintering temperature made it more porous than sample B [10].

The microstructure of sample C, which is illustrated in Figs. 13 and 15, shows that the 27R phase has a needle like morphology and other phases are distributed separately, consequently each phase can be oxidized separately. Optical micrographs of the polished section of sample C, after

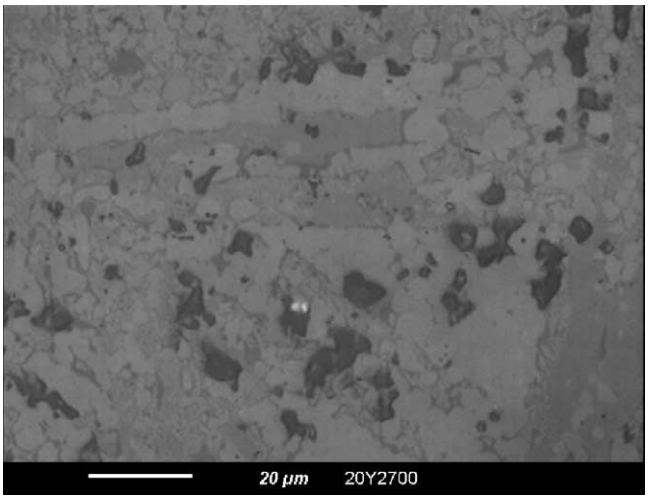

Fig. 13. Optical micrograph of polished section of the sample C.

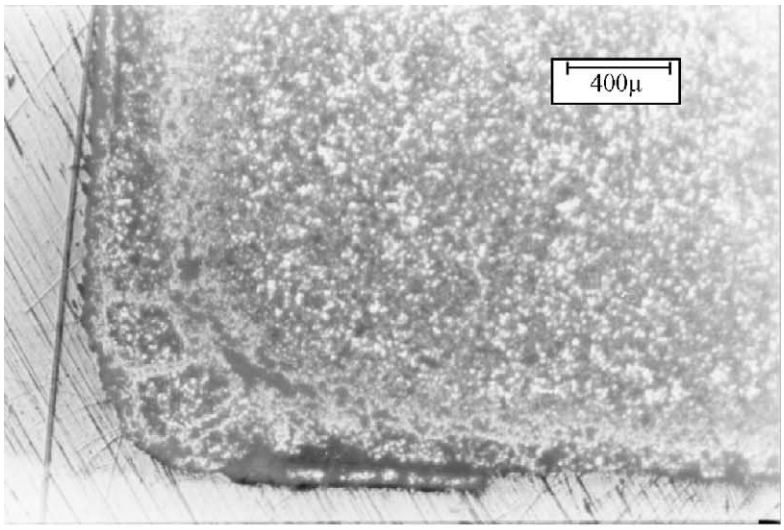

(a)

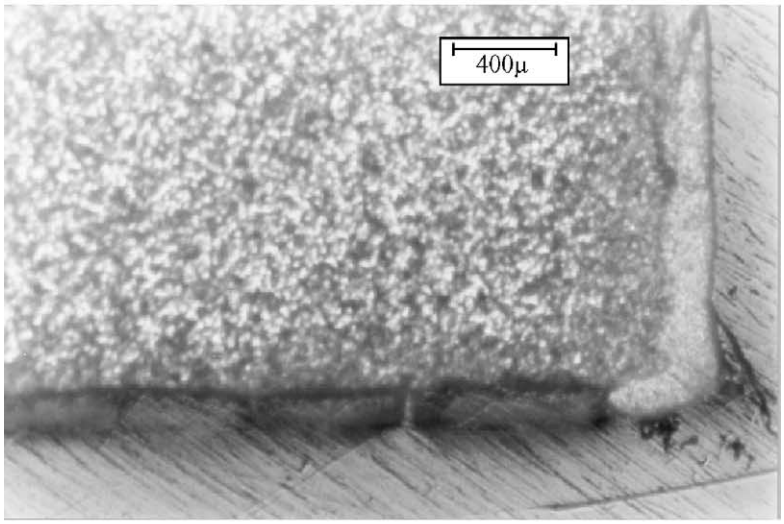

(b)

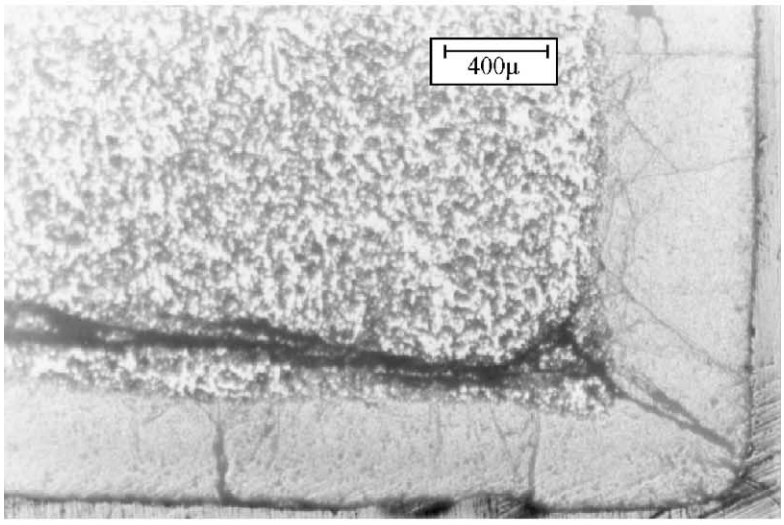

(c)

Fig. 14. Optical micrograph of polished section of the sample C oxidized at: (a) 1100 °C, 120 h, (b) 1300 °C, 12 h and (c) 1300 °C, 96 h.

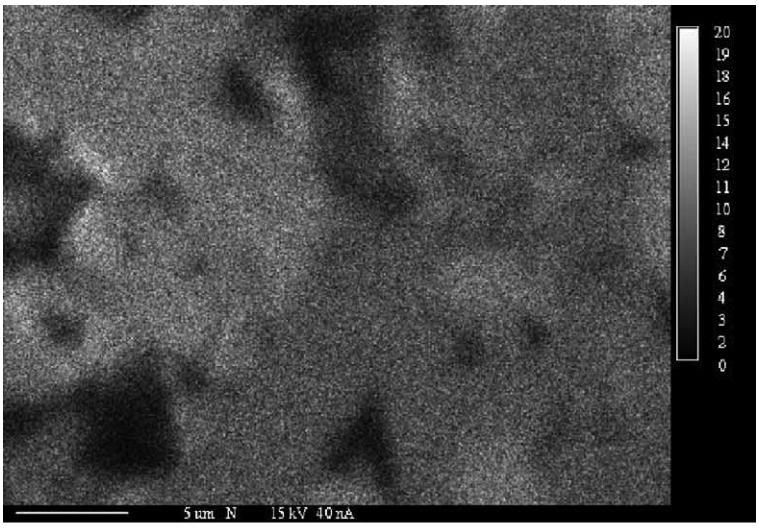

(a)

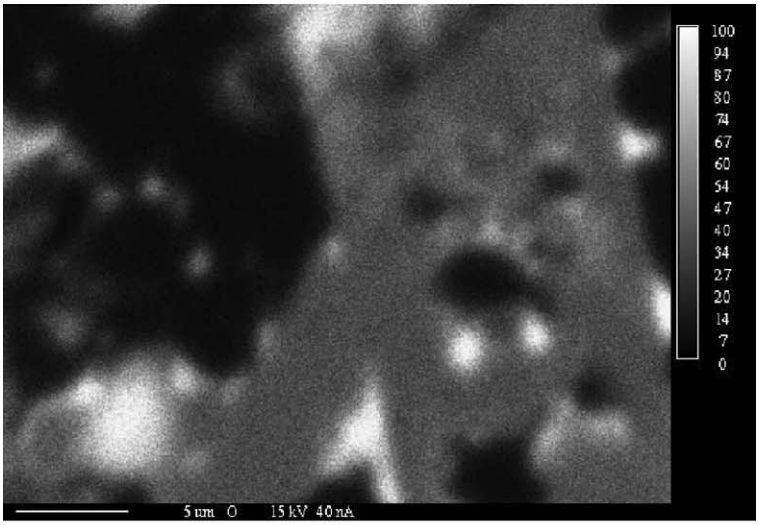

(b)

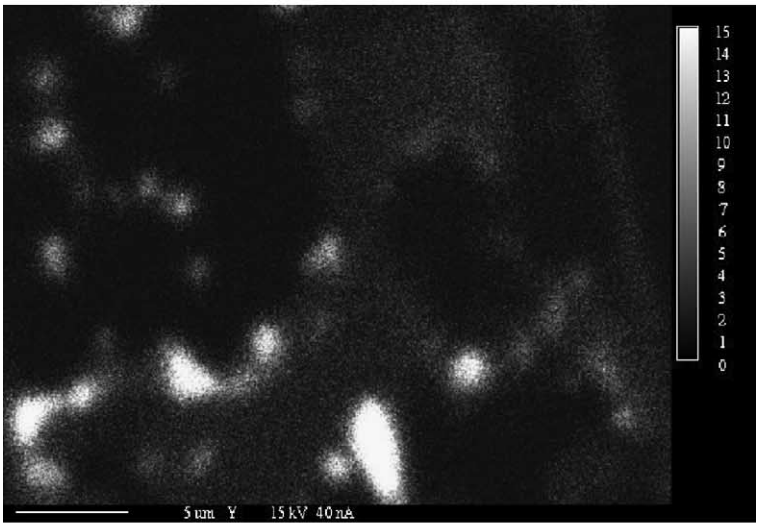

(c)

Fig. 15. WDS dot map of the sample C: (a) nitrogen map, (b) oxygen map and (c) yttrium map.

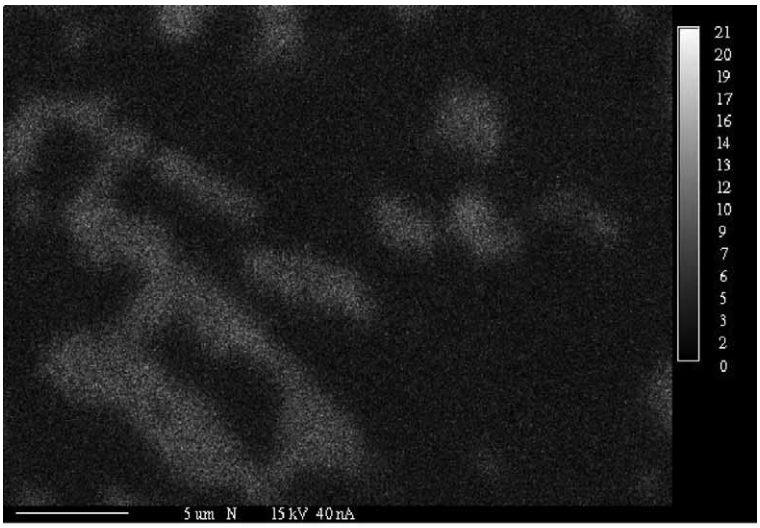

(a)

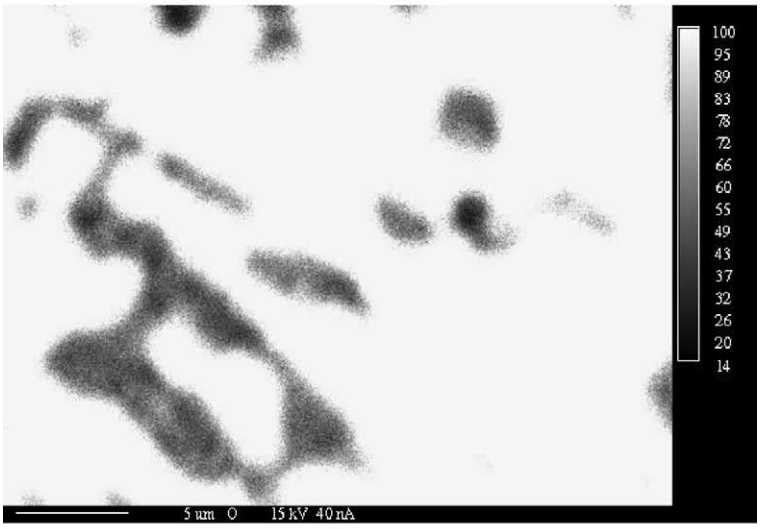

(b)

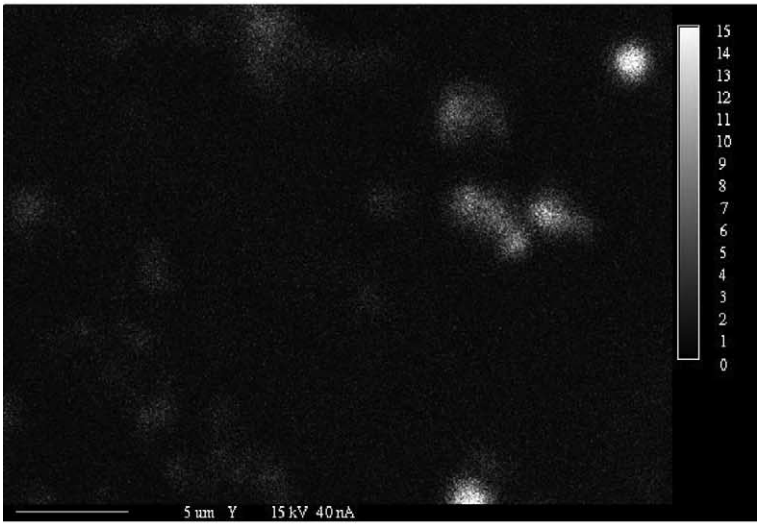

(c)

Fig. 16. WDS dot map of the sample D: (a) nitrogen map, (b) oxygen map and (c) yttrium map.

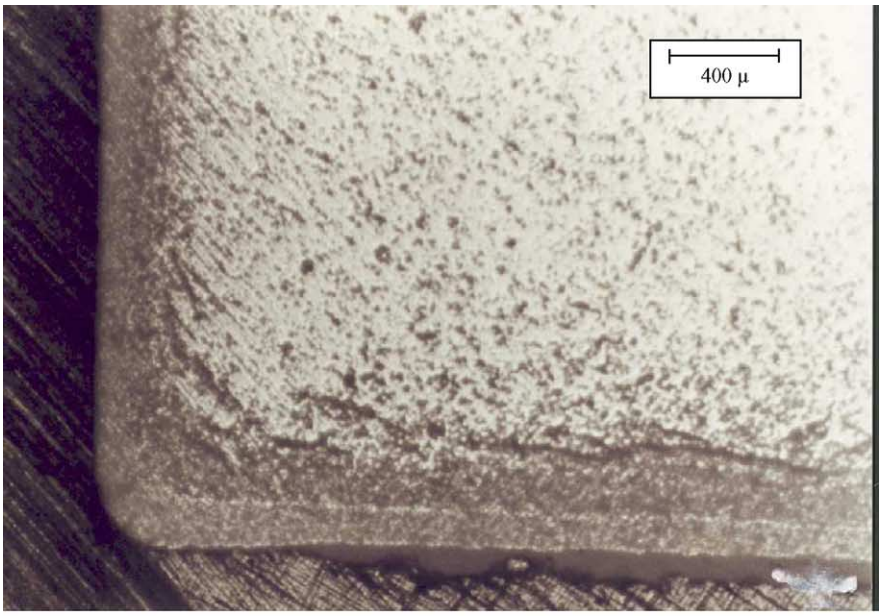

(a)

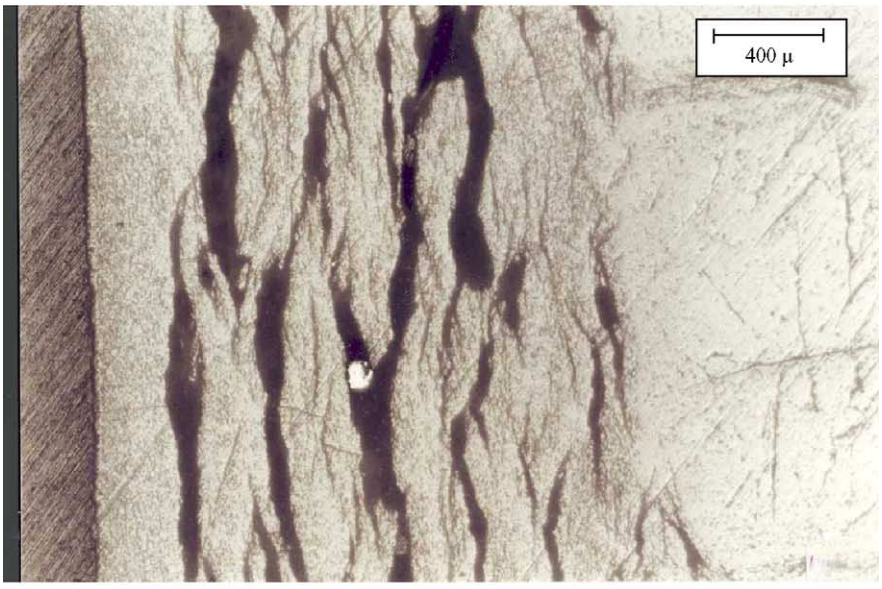

(b)

Fig. 17. Optical micrographs of polished section of sample D oxidized at 1300 °C: (a) 12 h, (b) 96 h.

oxidation at different temperatures and different exposure times, showed that a stable oxide layer has formed around the sample which its growth was controlled by time and temperature (Fig. 14).

Fig. 3c shows that, the weight gain versus exposure time of sample C is close to a linear rate-law. According to the results of Table 1, sample C is more porous than sample B and, such porosity can facilitate the transport of oxygen and nitrogen gas through the sample, therefore oxidation of this sample is accelerated.

The comparison of nitrogen X-ray maps of sample D (Fig. 16a and b) with the weight gain data (Fig. 3d) reveals that the γ-AlON phase, which is distributed as a continues phase around the AlN phase, is oxidized with a linear rate-law [11] and that controls the oxidation behavior of sample D.

Optical micrographs of polished section of sample D (Fig. 17) also show that, during the oxidation process an oxide layer is formed around the specimen but it cannot protect the specimen from further oxidation.

4. Conclusion

In the oxidation processes of AlN–AlON composites the finally obtained phase is alumina. The amount and distribu-

tion of AlN and AlON phases in samples control the oxidation behavior of such composites. In samples having high amount of AlN the high volume of the evolved nitrogen gas can crack the sample causing further oxidation.

In samples in which AlN, γ-AlON and 27R are distributed separately the resulting microstructure can provide a gradual exit of nitrogen gas. In such condition a protective alumina layer can form around the sample which can protect it from further oxidation.

References

[1] D. Robinson, R. Diekmann, Oxidation of aluminum nitride substrates, J. Mater. Sci. 29 (1994) 1949–1957.
[2] D. Suryanarayana, Oxidation kinetics of aluminum nitride, J. Am. Ceram. Soc. 73 (4) (1990) 1108–1110.
[3] H.E. Kim, A.J. Moorhead, Oxidation behavior of flexural strength of aluminum nitride exposed to air at elevated temperature, J. Am. Ceram. Soc. 77 (4) (1994) 1037–1041.
[4] A. Abid, R. Bensalem, B.J. Sealy, The thermal stability of AlN, J. Mater. Sci. 21 (1986) 1301–1304.
[5] P. Barthelme, The sintering and oxidation behavior of aluminum nitride, Eur. Ceram. 1 (1989) 1479–1483.
[6] A. Shimpo, M. Ueki, M. Naka, Mechanical properties of AlON-based composite ceramics at high temperature (part 1), effect of oxidation on mechanical properties of AlON–BN composite ceramics, J. Ceram. Soc. Jpn. 102 (2) (2001) 127–131.
[7] F. Fievez, P. Goeuriot, F. Thevenot, Oxidation kinetics of alumina—γ-aluminum oxynitride composites with Y_2O_3 or MgO sintering additives, in: R.J. Fordham (Ed.), High Temperature Corrosion of Technical Ceramics, Elsevier Applied Science, London.
[8] G.D. Quinn, N.D. Corbin, J.W. McCauley, Thermomechanical properties of aluminum oxynitride spinel, Am. Ceram. Soc. Bull. 63 (5) (1984) 723–730.
[9] N.D. Corbin, Aluminum oxynitride spinel: a review, J. Eur. Ceram. Soc. 5 (1989) 143–154.
[10] A. Maghsoudipour, F. Moztarzadeh, J.G. Heinrich, M.A. Bahrehvar, Sintering behavior of AlN–Al_2O_3 composites, Int. J. Eng. Sci. 13 (2) (2002) 159–167.
[11] M. Billy, The kinetics of gas–solid reaction and environmental degradation of nitrogen ceramics, in: F.L. Riley (Ed.), Progress in Nitrogen Ceramics, Martinus Nijhoff Publishers, Boston, 1983.